Nuclear Engineering and Technology 53 (2021) 932–941

Contents lists available at ScienceDirect

Nuclear Engineering and Technology

journal homepage: www.elsevier.com/locate/net

Original Article

Fracture simulation of SFR metallic fuel pin using finite element damage analysis method

Hyun-Woo Jung [a], Hyun-Kyu Song [a], Yun-Jae Kim [a, *], Dong-Wook Jerng [b]

[a] Korea University, Department of Mechanical Engineering, 145, Anam-ro, Sungbuk-gu, Seoul, 02841, South Korea
[b] Chung-ang University, Department of Energy Systems Engineering, 84, Heukseok-ro, Dongjak-gu, Seoul, 02841, South Korea

ARTICLE INFO

Article history:
Received 6 April 2020
Received in revised form
15 July 2020
Accepted 6 August 2020
Available online 18 August 2020

Keywords:
Sodium-cooled fast reactor
Metallic fuel
Fracture simulation
Failure prediction

ABSTRACT

This paper suggests a fracture simulation method for SFR metallic fuel pin under accident condition. Two major failure mechanisms - creep damage and eutectic penetration - are implemented in the suggested method. To simulate damaged element, stress-reduction concept to reduce stiffness of the damaged element is applied. Using the proposed method, the failure size of cladding can be predicted in addition to the failure time and failure site. To verify the suggested method, Whole-pin furnace (WPF) test and TREAT-M test conducted at Argonne National Laboratory (ANL) are simulated. In all cases, predicted results and experimental results are overall in good agreement. Based on the simulation result, the effect of eutectic-penetration depth representing failure behavior on failure size is studied.

1. Introduction

Sodium-cooled fast reactor (SFR) is a promising Gen IV fast reactor that has superior safety features resulting from high thermal conductivity, low corrosiveness and high boiling temperature of sodium coolant [1]. Furthermore, SFR using metallic fuels has additional safety features resulting from high conductivity of the fuel [2]. Despite safety features, severe accident in metal-fuelled SFR could happen when multiple transient events happen simultaneously [1,2]. Thus it is important to predict possible accident sequences of severe accident for safe operation of SFR.

When the severe accident occurs, fuel temperature increases, and partial melting of the fuel can occur. Due to creep damage and eutectic penetration, cladding can fail, and molten fuel can be ejected into the sodium channel [3,4]. It is reported that in-channel behavior of the molten fuel can be affected by pressure, the mass of molten fuel and failure site/size [5–7]. To predict the accident sequences involving recriticality and channel blockage, it is important to predict failure time, site and size.

Some analysis codes have been developed to predict cladding failure; SAS4A-FPIN [8], LIFE-METAL [9] by Argonne national laboratory and FEAST-METAL [10] by Massachusetts institute of technology. Two major failure mechanisms – creep damage and eutectic penetration – were implemented to these codes but failure size cannot be predicted using these codes. However, prediction of the failure size is quite important because the coolability of the ejected fuel debris is affected by the failure size [6], which is highly related to the possibility of recriticality and complete disruption of core structure. Summary of failure prediction codes is suggested in Table 1.

In this paper, a method to predict cladding failure via finite element (FE) damage analysis using a stress-reduction concept is presented. Failure size can be predicted by proposed method, as well as failure time and failure site. For FE analysis, commercial FE program, Abaqus [11], is used. To verify the presented method, published experimental data (Whole-pin furnace test [12–14] and TREAT-M test [4,15,16]) are simulated and simulation results are compared with the experimental data. Furthermore, based on the simulation result, the effect of eutectic-penetration depth representing failure behavior on failure size is studied.

2. Cladding failure simulation method

2.1. Fracture simulation procedure

The cladding failure simulation method used in this work consists of the following four steps. The first step is steady-state heat transfer analysis to determine temperature distributions in the pre-

* Corresponding author.
E-mail address: kimy0308@korea.ac.kr (Y.-J. Kim).

https://doi.org/10.1016/j.net.2020.08.009

Nomenclature

SFR	sodium-cooled fast reactor
CDF	cumulative damage fraction
WPF	Whole-pin furnace
ω_{creep}	creep damage fraction
ω_{FCCI}	eutectic penetration damage fraction
h_{conv}	convective heat transfer coefficient
Nu	Nusselt number
Pe	Peclet number
φ	fast neutron flux
q'''	volumetric heat generation rate
dX/dt	eutectic penetration rate
X	eutectic penetration depth
x	local eutectic penetration depth
L_e	element size
T	temperature
t_{rup}	creep rupture time

Table 1
Existing cladding failure prediction codes.

	LIFE-METAL [9]	SAS4A-FPIN2 [8]	FEAST-METAL [10]	This study
1D/2D	1D	2D Axisymm.	1D	2D Axisymm.
Eutectic penetration model	Empirical correlation	Empirical correlation	Diffusion model based on precipitation kinetics	Empirical correlation
Creep fracture model	Cumulative damage fraction (CDF)	Cumulative damage fraction (CDF)	Cumulative Damage Fraction (CDF) Constrained diffusional cavity growth Model	Cumulative damage fraction (CDF)
Analytically predictable result	Failure time Failure site	Failure time Failure site	Failure time Failure site	Failure time Failure site Failure size

accident state. In the steady-state heat transfer analysis, fast neutron fluence is calculated based on power distribution to reflect the effect of neutron-irradiation on cladding mechanical properties. The second step is transient-state heat transfer analysis to determine temperature distribution in the accident state. The transient-state heat transfer analysis is conducted based on fuel power distribution, coolant flow rate and coolant temperature determined from accident (or test) conditions. The third step is calculation of the eutectic penetration rate using commercial FE software Abaqus with a post-processing program. The eutectic penetration rate is calculated from the inner surface temperature of the cladding during the accident state. The final step is stress analysis to predict cladding failure. Steady-state and transient temperature distributions and plenum pressure history is applied to calculate stresses. Creep damage fraction is calculated from stress and temperature information in all analysis steps. Based on the creep damage fraction and the eutectic penetration depth calculated using a post-processing program, element failure is determined and simulated using a stress-reduction technique implemented in Abaqus [11]. The flowchart of the suggested fracture simulation method is shown in Fig. 1 and detail descriptions of each analysis steps are given in the subsequent sub-sections.

2.2. Heat transfer analysis

Heat transfer analysis was conducted to calculate temperature distribution of cladding from fuel power distribution, coolant

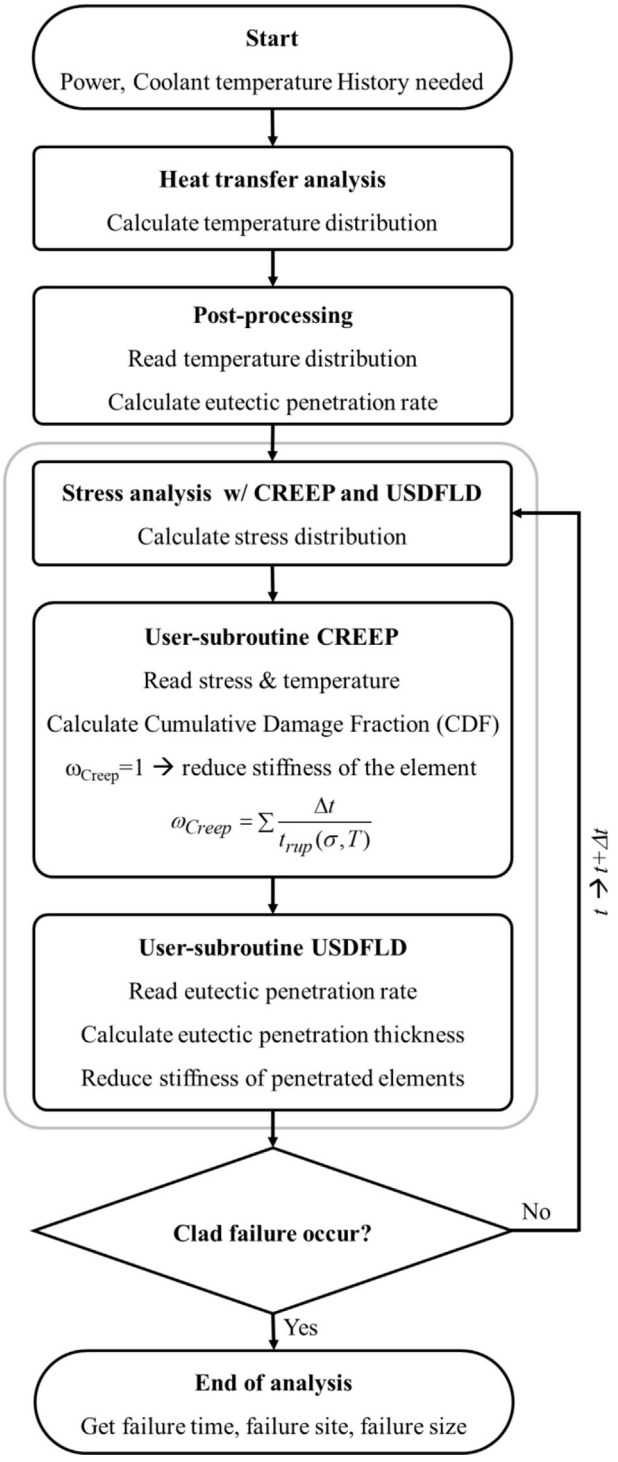

Fig. 1. Flowchart of present fracture simulation method.

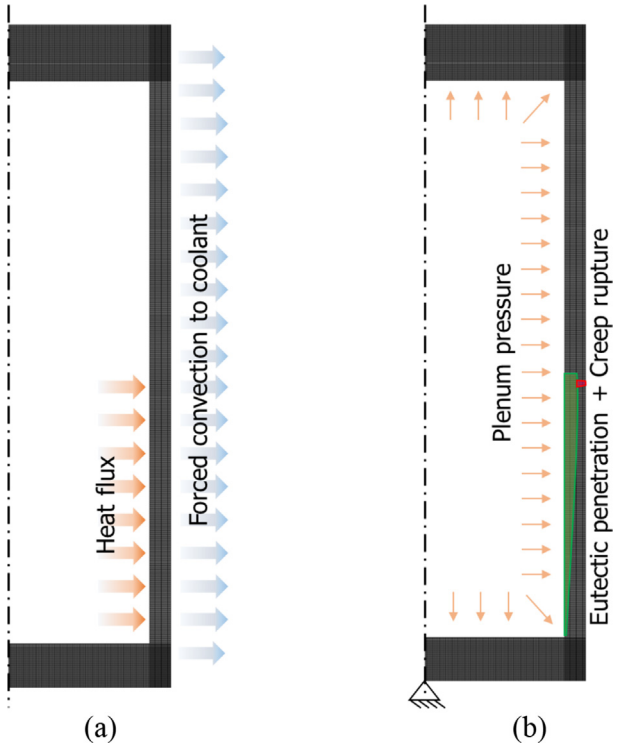

Fig. 2. Boundary conditions (a) for heat transfer analysis and (b) for Stress analysis.

temperature and flow-rate in the steady-state or transient-state condition. It was assumed that heat transfer analysis results are not affected by deformation of cladding.

Transient heat transfer analysis method, *HEAT TRANSFER, supported in Abaqus [11] was used. Finite element mesh with thermal boundary condition is shown in Fig. 2(a). Two-dimensional axisymmetric quadratic heat transfer element, DCAX8, was used. The element size was set to be 1.0 mm to the longitudinal direction and 0.0127 mm to the radial direction. Sensitivity analysis on element type and element size was conducted, of which the results will be discussed later in Section 3.2.

To apply fuel power as heat flux to the inner surface of cladding, the user-subroutine DFLUX supported in Abaqus [11] is used. To simulate published experimental tests (WPF and TREAT-M tests), the axial power distribution of IFR fuel [10] was applied. To apply forced convection to the outer surface of cladding, the user-subroutine FILM supported in Abaqus [11] was used. Convective heat transfer coefficient was calculated at each surface integration points using the Schad-modified correlation [17]:

$$h_{conv}=\frac{\pi r_{co}k_{Na}}{2\sqrt{3}(r_{co}+r_w)^2-\pi r_{co}^2-\pi r_w^2}\left[\frac{4\bar{m}c_{p,Na}}{k_{Na}(\pi r_{co}+\pi r_w)}\right]^{0.3}\left[-8.075+12.48\left(1+\frac{r_w}{r_{co}}\right)-4.275\left(1+\frac{r_w}{r_{co}}\right)^2\right] \quad \text{Eq. (1)}$$

h_{conv} is convective heat transfer coefficient in $W/m^2/K$, k_{Na} is sodium conductivity in $W/m/K$, $C_{p,Na}$ is specific heat of sodium in $J/kg/K$, r_{co} is outer radius of cladding in m, r_w is wire radius in m and $\bar{m}$ is mass flow rate of sodium in kg/s.

To implement the neutron-irradiation effect on creep and swelling, fast neutron fluence was calculated based on the following equations using the user-subroutine USDFLD [11]:

$$\varphi = 840000q''' \quad \text{Eq. (2)}$$

φ is fast neutron flux in $n/cm^2/s$ and q''' is volumetric heat generation rate in W/m^3.

Thermal material properties of claddings (HT9, D9, 316SS) and sodium from literatures are used in this work: thermal conductivity [18,19], specific heat [19–21], and enthalpy [19].

2.3. Stress analysis

Stress distribution was calculated from calculated temperature distribution and plenum pressure, from which cladding failure was predicted considering creep damage and eutectic penetration. Finite element modelling and kinematic boundary condition is shown in Fig. 2(b).

To investigate stress states in cladding as a function of time, quasi-static analysis method, *VISCO supported by Abaqus, was used [11]. Two-dimensional axisymmetric quadratic structural element with reduced-integrations (CAX8R in Abaqus) was used. The same element size as that in the heat transfer analysis was used; 1 mm in the axial direction and 0.0127 mm in the radial direction.

To apply the plenum pressure history, the user-subroutine DLOAD in Abaqus was used. Creep strain rate and creep damage fraction due to the fast neutron fluence were calculated using the user-subroutine CREEP. Eutectic penetration rate was transferred from a post-processing program, and penetrated elements were determined using the user-subroutine USDFLD. Detail description of simulation methods of eutectic penetration and creep damage will be explained later in Sections 2.4 and 2.5, respectively.

Mechanical properties of claddings (HT9, D9, 316SS) from literatures are used in this work: elastic modulus [22], poisson's ratio [22], thermal expansion coefficient [18], creep strain rate [8], creep rupture time [23–25] and swelling strain [26].

2.4. Simulation method of eutectic penetration

The uranium constituent in the metallic fuel interacts metallurgically with the iron constituent in the cladding at elevated temperature. Wall-thinning of cladding results from the eutectic reaction between the uranic fuel and the ferrous cladding. The

eutectic reaction was implemented using following equation of eutectic penetration rate given in SAS4A [8,27]:

$$\frac{dX}{dt}=\begin{cases}0 & T<1353K\\ 922+2.93(T-1388)-0.215(T-1388)^2+0.001134(T-1388)^3 & 1353\mathrm{K}\le T<K\\ \exp\left(22.85-\dfrac{27624}{\mathrm{T}}\right) & T\ge 1506K\end{cases} \quad \text{Eq. (3)}$$

dX/dt is penetration rate in $\mu m/s$ and T is temperature in K. In Eq. (3), the critical temperature of the eutectic penetration is defined as 1353 K. At the temperature lower than the critical temperature, the penetration rate is set to zero.

Note that Eq. (3) can be used for short-term accidents accompanying rapid temperature rise but cannot be used for long-lasting accidents which cause relatively slow temperature rise. In such cases, Cohen et al. [28,29] suggested the following equation of eutectic penetration rate based on the experimental result at 923 K–1043 K in Alpha gamma hot cell facility (AGHCF):

$$\frac{dX}{dt}=\exp\left(11.646-\frac{15865}{T}\right) \quad \text{Eq. (4)}$$

In this paper, the following equation combining Eq. (3) with Eq. (4) is used:

$$\frac{dX}{dt}=\begin{cases}0 & T<948K\\ \exp\left(11.646-\dfrac{15865}{T}\right) & 948K\le T<1353K\\ 922+2.93(T-1388)-0.215(T-1388)^2+0.001134(T-1388)^3 & 1353K\le T<1506K\\ \exp\left(22.85-\dfrac{27624}{T}\right) & T\ge 1506K\end{cases} \quad \text{Eq. (5)}$$

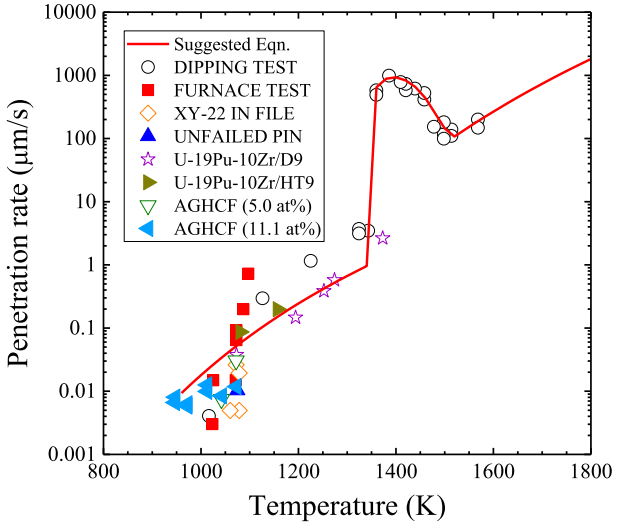

Fig. 3. Assumed eutectic penetration rate between uranic fuel and ferrous cladding, compared with published experimental data [8,27–29].

Fig. 3 compares published experimental data with Eq. (5).

The method of simulating eutectic penetration is schematically shown in Fig. 4. Eutectic penetration rate is calculated from inner surface temperature of cladding using post-processing program and transferred to Abaqus solver. The penetration damage fraction of the element is calculated at the integration point using the following equation:

$$\omega FCCI=\frac{x}{L_e} \quad \text{Eq. (6)}$$

ω_{FCCI} is penetration damage fraction, x is local penetration depth and L_e is element size. When all gauss points within an element fail, the element is deleted by reducing all stress components and behaves like a void. Such stress-reduction technique has been used in ductile fracture simulation [30] and creep crack growth simulation [31].

2.5. Creep damage calculation

Under transient conditions, creep rupture of cladding can be calculated using cumulative damage fraction (CDF) [8,27]:

$$\omega_{Creep}=\sum\frac{\Delta t}{t_{rup}(\sigma,T)} \quad \text{Eq. (7)}$$

where ω_{Creep} is creep damage fraction, Δt is time increment, t_{rup} is the creep rupture time, σ is effective stress and T is temperature. Cumulative damage fraction is calculated at the integration point in all analysis steps. When the cumulative damage fraction becomes unity, all stress components were reduced to zero, as described in Section 2.4.

For the creep rupture time $t_{rup}(\sigma,T)$ in Eq. (7), the models in SAS4A DEFORM5 [23–25] were used for HT9, 316SS and D9. The creep rupture time model for HT9 is dependent only on the equivalent stress and temperature, while those for 316SS and D9 depend on the stress, temperature and irradiation dose.

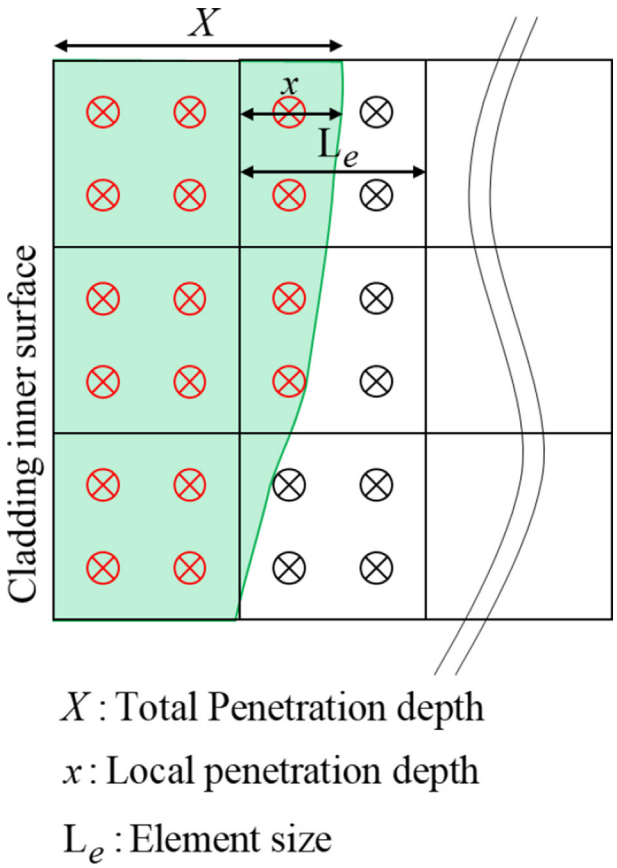

Fig. 4. Schematic illustration of simulating eutectic penetration.

Table 2
Design parameters of WPF test pins [12–14].

Fuel length	343 mm
Fuel radius	2.2 mm
Clad inner radius	2.54 mm
Clad outer radius	2.92 mm
Plenum to fuel volume ratio	1.0 (FM1, FM2, FM6) 1.4 (FM3) 1.5 (FM4, FM5)
Bond sodium above fuel level	6.35 mm

3. Fracture simulation of Whole-pin furnace test

3.1. Test description

To verify the cladding failure simulation method proposed in this work under extended transients, WPF tests are simulated. The WPF test was out-of-pile heating test where irradiated pins were exposed at 650 °C–820 °C for a few to thousands of minutes [12–14]. The purpose of WPF test was to prove safety features of metallic fuels and to verify analysis codes under extended transient condition. Design parameters of WPF test pins are given in Table 2 and results of simulated test cases are summarized in Table 3. The source of irradiated fuel pins was the Experimental Breeder Reactor II (EBR-II). In this work, steady-state pre-irradiating condition in EBR-II is simulated using X425 benchmark condition [10,32,33] to calculate cumulative damage fraction (CDF) and fast neutron fluence of the irradiated fuel pins. For simulation, temperature distribution from experiment and plenum pressure calculated via the FEAST-M analysis code given in Table 3 are applied. Simulation results of WPF tests are given in Table 4 and compared with the results obtained from SAS4A, LIFE and FEAST codes.

3.2. Results for the test FM1, FM2 and FM3

The FM1, FM2 and FM3 tests were low-burnup pin tests with similar pressure and temperature conditions. Despite of their similar test conditions, failure times were largely different, as given in Table 3; the failure times of FM1, FM2 and FM3 tests were 67 min, 112 min and 146 min, respectively. Such large deviation of failure time might results from large deviation of the eutectic penetration rate; the average eutectic penetration rates of the FM1, FM2, and FM3 tests were found to be 3.62 μm/min, 2.26 μm/min, and 1.72 μm/min. Predicted cladding failure times of FM1, FM2, and FM3 tests from present FE analysis using Abaqus are 84 min, 80 min, and 90 min. Predicted failure sites are fuel top regions and these results are agrees with experimental results. Among three experimental cases, the failure size of FM2 is available only. Experimental axial failure size of FM2 pin is 2.0 mm and predicted axial failure sizes of FM1, FM2 and FM3 are 1.0 mm, 3.0 mm and 3.0 mm. Circumferential failure size cannot be derived using our FE analysis method because we used axisymmetric model. Predicted peak strain is lower than experimental peak strain because our model cannot simulate local strain concentration caused by instability as given in Table 4.

Low-burnup pins such as FM1, FM2 and FM3 pins have low plenum pressure, so that creep-driving force is low. Therefore, for the low-burnup pins, failure occurs after most of cladding wall penetrated. Experimental results of FM1, FM2 and FM3 pins shows 64%, 67% and 65% of penetration at failure. FE analysis results show similar tendency to the experimental result, as shown in Fig. 5. Predicted penetrated fraction of cladding wall at failure of FM1, FM2 and FM3 pins are 82%, 76% and 90%.

Sensitivity analysis on element type and size is conducted and the results are suggested in Table 5. There is large difference in predicted failure time between 4-node elements (CAX4, CAX4R) and 8-node elements (CAX8, CAX8R). This difference is caused by inaccurate eutectic penetration rate of 4-node element. Applied eutectic penetration rate is as lower as 35% than Cohen equation

Table 3
Summary of WPF test [12–14].

Case	Fuel	Clad	Burnup	Peak temperature[a]	Peak plenum pressure[b]	Duration	Failure
FM1	U-10Zr	HT9	3.0 at%	810 °C, 820 °C	2.85 MPa	67 min	O
FM2	U-19Pu-10Zr	HT9	3.0 at%	810 °C, 820 °C	3.43 MPa	112 min	O
FM3	U-26Pu-10Zr	HT9	2.2 at%	810 °C, 820 °C	1.72 MPa	146 min	O
FM4	U-19Pu-10Zr	HT9	11.4 at%	750 °C, 770 °C	9.22 MPa	68 min	O
FM5	U-19Pu-10Zr	HT9	11.4 at%	780 °C, 870 °C	9.27 MPa	3 min	X
FM6	U-19Pu-10Zr	HT9	11.3 at%	650 °C, 670 °C	13.35 MPa	2160 min	X

[a] Maximum temperature of external surface temperature of clad at fuel top and clad top.
[b] Peak plenum pressure estimated by FEAST-M [10].

Table 4
Summary of cladding failure simulation results of WPF tests [10,14].

Failure Time (min)	**Case**	**Exp.**	**SAS4A**	**LIFE**	**FEAST**[a]	**This study**
	FM1	67	36	79	69/58	84
	FM2	112	42	75	56/48	80
	FM3	146	108	217	129/110	90
	FM4	68	16	9	12/10	54
	FM5	N/A	N/A	N/A	N/A	N/A
	FM6	N/A	222	1320	N/A	681
Failure site	**Case**	**Exp.**	**SAS4A**	**LIFE**	**FEAST**[a]	**This study**
	FM1	Fuel top	Fuel top	Fuel top	Fuel top	Fuel top
	FM2	Fuel top	Fuel top	Fuel top	Fuel top	Fuel top
	FM3	Fuel top	Fuel top	Fuel top	Fuel top	Fuel top
	FM4	Plenum	Fuel top	Fuel top	Fuel top	Fuel top
	FM5	N/A	N/A	N/A	N/A	N/A
	FM6	N/A	Fuel top	Fuel top	N/A	Fuel top
Eutectic penetration (%)	**Case**	**Exp.**	**SAS4A**	**LIFE**	**FEAST**[a]	**This study**
	FM1	64	30	53	51/47	82
	FM2	67	37	50	45/42	76
	FM3	65	86	50	70/64	90
	FM4[b]	24	8.2	3	10/10	28
	FM5[c]	0	0.15	0	5/5	0.26
	FM6[c]	0	0	0	5/5	0
Peak strain near failure site (%)	**Case**	**Exp.**	**SAS4A**	**LIFE**	**FEAST**[a]	**This study**
	FM1	3.3	6	1.1	0.7/0.5	1.1
	FM2	4.3	6	1	0.7/0.5	1.1
	FM3	1.2	6	1	0.7/0.4	1.0
	FM4	15	15	0.7	0.4/0.3	1.2
	FM5[c]	0.1	0.6	0	0.2/0.2	0.5
	FM6[c]	0.89	4.5	1	1/1	1.0
Failure size[d] **(mm)**	**Case**	**Exp.**	**SAS4A**	**LIFE**	**FEAST**	**This study**
	FM1	N/A	N/A	N/A	N/A	1.0/-
	FM2	2.0/0.9				3.0/-
	FM3	N/A				3.0/-
	FM4	12.5/3.5				5.5/-
	FM5	N/A				N/A
	FM6	N/A				2.5/-

[a] Failure criteria (Cumulative damage fraction/Constrained diffusional cavity growth).
[b] Penetration depth at fuel top.
[c] Maximum value.
[d] Axial size (length)/circumferential size (width).

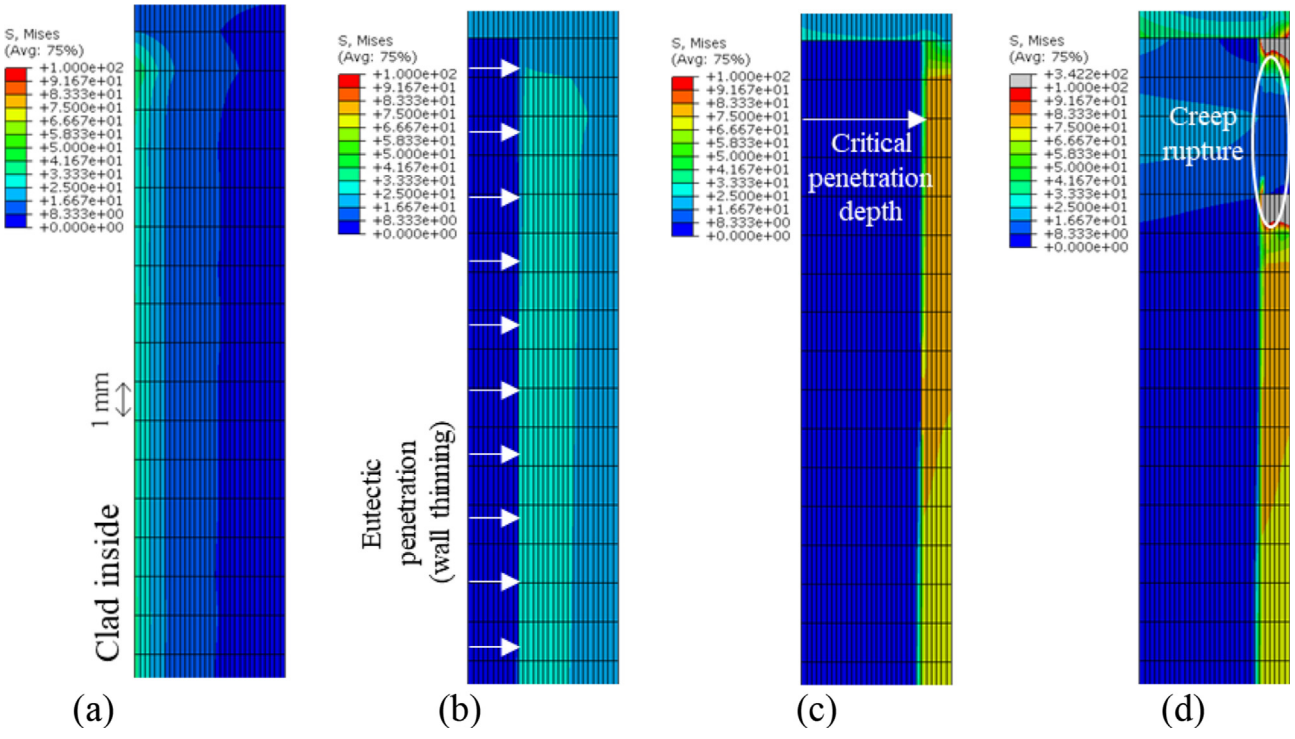

Fig. 5. Stress analysis results of FM2 test: (a) 623 s, (b) 2971 s, (c) 5051 s and (d) 5059 s.

Table 5
Element sensitivity analysis result (FM1).

	Case	Failure time (min)	Failure site – Axial location (%)	Eutectic penetration (%)	Peak strain (%)	Failure size (mm)
Element type	CAX4	129	99.1	79.6	1.037	1.5
	CAX4R	128	99.4	78.9	1.036	1.0
	CAX8	84	99.4	81.2	1.063	1.0
	CAX8R	84	99.4	81.7	1.056	1.0
Axial element size	6 mm	83	98.3	79.9	1.039	3.0
	2 mm	83	99.4	80.6	1.069	1.0
	1 mm	84	99.4	81.7	1.056	1.0
	0.6 mm	85	99.5	81.9	1.054	0.9
	0.3 mm	85	99.4	81.8	1.044	1.05
# Radial element	10	85	99.4	82.4	1.052	2.0
	20	85	99.4	81.9	1.053	1.0
	30	84	99.4	81.7	1.056	1.0
	60	84	99.4	81.7	1.061	1.5

Table 6
Design parameters of TREAT-M test pins [4].

	EBR-II driver fuel	IFR type
Fuel	U-5Fs	U-19Pu-10Zr
		U-10Zr
Clad material	316 SS	D9
		HT9
Fuel mass	52 g	78 g
Fuel length	343 mm	343 mm
Fuel radius	1.65 mm	2.16 mm
Clad inner radius	1.905 mm	2.54 mm
Clad outer radius	2.21 mm	2.92 mm
Plenum length	193 mm	246 mm
Bond sodium above fuel level	28 mm	6.35 mm

Table 7
Summary of TREAT-M test [4].

Case	Fuel	Clad	Burnup	Peak P/F[a]	Peak pressure	Failure
M2(1)	U-5Fs	316 SS	0.3 at%	4.1	0.7 MPa	X
M2(2)	U-5Fs	316 SS	4.4 at%	4.2	7–9 MPa	O
M2(3)	U-5Fs	316 SS	7.9 at%	4.1	17–20 MPa	O
M3(1)	U-5Fs	316 SS	0.3 at%	4.1	0.7 MPa	X
M3(2)	U-5Fs	316 SS	4.4 at%	4.0	7–9 MPa	X
M3(3)	U-5Fs	316 SS	7.9 at%	3.4	17–23 MPa	X
M6(1)	U-19Pu-10Zr	D9	1.9 at%	4.6	3 MPa	X
M6(2)	U-19Pu-10Zr	D9	5.3 at%	4.5	10 MPa	O
M7(1)	U-19Pu-10Zr	D9	9.8 at%	4.0	19 MPa	O
M7(2)	U-10Zr	HT9	2.9 at%	4.8	6 MPa	X

[a] Power over coolant flow rate normalized by the value of steady-state condition (43 kW/m, 630 K inlet, 780 K outlet coolant temperature) In case that failure did not occur, peak P/F indicates maximum P/F.

[28]. On the other hand, there is not notable error in predicted failure site, penetration depth, strain and failure size. Hence, most accurate and efficient 8-node reduced-integration element (CAX8R) is used for following simulations. Axial and radial size of element do not affect failure time, failure site, penetration depth, and strain as shown in Table 5. There is notable error in failure size when axial element size is 6.0 mm; estimated failure size is 3.0 mm which is 3 times larger than other results. This error arises from low resolution of failure size caused by large element size. When using CAX8R element with 6 mm of axial length, the resolution of failure size becomes 3 mm. Because the resolution should be smaller than failure size, element with 1 mm of axial length is used for the following simulations. Radial size of element has effect on failure size by affecting creep damage propagation process but there is not meaningful tendency. Considering efficiency, 30 numbers of radial elements is used for the following simulations.

3.3. Result for the test FM4

FM4 test is high-burnup pin test. Initial plenum pressure of FM4 pin is 7 MPa, which is far larger than low-burnup pins. In test, because of large plenum pressure, cladding expanded largely and contacted with shield wall [14]. The contact between cladding and shield wall resulted in delay of failure and failure site shifted from fuel top to plenum [14]. Experimental failure time of FM4 pin is 68 min and predicted failure time is 54 min. Predicted failure site is fuel top region and axial failure size is 5.5 mm. Experimental penetrated fraction of cladding wall at fuel top region is 24% and predicted penetrated fraction of cladding wall at fuel top region is 28%. Experimental peak strain near failure site (plenum) is 15%, which is far larger than predicted peak strain near failure site (fuel top), 1.2%.

Creep damage is major failure mechanism of high-burnup pin. Because of high pressure causing high stress, creep damage initiates when penetration depth is low. Because the time from creep damage initiation to complete failure is relatively longer than that of low-burnup pin, creep damage axially propagates further and failure size becomes larger. Predicted failure size is 5.5 mm and it is at least 1.8 times larger than that of low-burnup pin.

3.4. Result for the test FM5 and FM6

FM5 test simulated EBR-II Mark-V UN-1 loss of flow (LOF) event [14]. Like actual LOF transient condition, the FM5 test lasted for short time – about 3 min. Cladding failure does not occur in both experiment and FE analysis. Eutectic penetration was not observed in the test and predicted eutectic penetration depth is 0.988 μm (0.26% of cladding wall).

FM6 test is high-burnup pin test. Initial plenum pressure is 11 MPa and peak temperature is 650 °C–670 °C, which is lower than that of other tests. The FM6 test lasted for 2160 min and failure did not occur. Predicted failure time is 681 min. This error is caused by the creep rupture property of HT9; because of low temperature, eutectic penetration does not occur in both experiment and FE analysis. The creep rupture property applied to our model is identical to that of SAS4A-FPIN, which is short-term creep rupture property [14]. It makes conservative prediction result for long-term creep condition like FM6 test condition.

4. Fracture simulation of treat-M test

4.1. Test description

To verify the cladding failure simulation method proposed in this work under severe accident condition, TREAT-M tests are simulated. The TREAT-M test is in-pile simulated experiment of

Table 8
Summary of cladding failure simulation results of TREAT-M tests [4].

	Case	Experiment	COBRA/EXP	This study
Peak P/F[a]	M2(1)	4.1 [X]	4.7	5.6
	M2(2)	4.2 [O]	4.5	5.6
	M2(3)	4.1 [O]	3.6	4.1
	M3(1)	4.1 [X]	4.8	5.8
	M3(2)	4.1 [X]	4.4	5.7
	M3(3)	3.4 [X]	3.6	3.8
	M6(1)	4.4 [X]	4.6	4.4
	M6(2)	4.4 [O]	4.5	4.3
	M7(1)	4.0 [O]	4.4	4.5
	M7(2)	4.8 [X]	4.4	4.6
Eutectic penetration (%)	M2(1)	N/A	N/A	100
	M2(2)	N/A		86
	M2(3)	0		0
	M3(1)	N/A		100
	M3(2)	N/A		83
	M3(3)	N/A		0
	M6(1)	N/A		100
	M6(2)	N/A		87
	M7(1)	N/A		0
	M7(2)	30		39
Failure size (mm)	M2(1)	N/A	N/A	33.0
	M2(2)	N/A		0.5
	M2(3)	N/A		0.5
	M3(1)	N/A		18.0
	M3(2)	N/A		1.0
	M3(3)	N/A		1.0
	M6(1)	N/A		20.5
	M6(2)	3.8<		1.5
	M7(1)	N/A		1.5
	M7(2)	N/A		7.0
Peak temperature at failure (K)	M2(1)	N/A	N/A	1379
	M2(2)			1372
	M2(3)			1247
	M3(1)			1383
	M3(2)			1376
	M3(3)			1217
	M6(1)			1383
	M6(2)			1378
	M7(1)			1333
	M7(2)			1365

[a] Experimental peak P/F is given with whether failure occurred or not ([O]: failed and [X]: not failed).

transient overpower (UTOP) accident [4,15,16]. The power of pre-irradiated fuel pin was increased exponentially to imitate UTOP accident. The degree of overpower is represented by power over coolant flowrate, P/F. The design parameters of fuel pins used for the tests are given in Table 6. There are 4 test cases with 10 pre-irradiated fuel pins: M2(1–3), M3(1–3), M6(1–2), M7(1–2). Test summary of TREAT-M tests is given in Table 7. Power, coolant temperature, and plenum pressure histories are given in literatures [4,15,16]. The source of irradiated fuel pins was the Experimental Breeder Reactor II (EBR-II). In this work, steady-state pre-irradiating condition in EBR-II is simulated using X425 benchmark condition [10,32,33] to calculate cumulative damage fraction (CDF) and fast neutron fluence of the irradiated fuel pins. Simulation results of TREAT-M tests are given in Table 8 and compared with the results obtained from COBRA/EXP codes.

4.2. Result for the test M2 and M3

M2 and M3 tests are simulated experiments of overpower condition with U-5Fs fuel and 316 SS cladding. Three fuel pins with different burnups were exposed to the hypothetical overpower condition simultaneously: 0.3 at% (M2(1) and M3(1)), 4.4 at% (M2(2) and M3(2)) and 7.9 at% (M2(3) and M3(3)). M3 test was stopped just before failure; peak P/F value was derived from M2 test result [4].

M2(1) and M3(1) test pins are low-burnup (0.3 at%) pins. Initial plenum pressure is 0.45 MPa. Experimental peak P/F of both tests is 4.1 and failure did not occur. Predicted P/Fs at failure of M2(1) and M3(1) tests are 5.6 and 5.8, respectively. In FE analysis result, creep damage is not observed because of low plenum pressure. In these cases, cladding failure arises from rapid eutectic penetration, which occurs at temperature above eutectic critical temperature, 1353 K. Peak temperature at failure of M2(1) and M3(1) tests are 1379 K and 1383 K, as given Table 8. Predicted axial failure sizes of M2(1) and M3(1) tests are 33.0 mm and 18.0 mm, respectively.

M2(2) and M3(2) test pins are medium-burnup (4.4 at%) pins. Initial plenum pressure is 4.52 MPa. Experimental peak P/Fs of M2(2) and M3(2) tests are 4.2 and 4.1, respectively. In M2(2) test, unexpected failure occurred because of temperature oscillation caused by wire-wrap [4]. Predicted P/Fs at failure of M2(2) and M3(2) tests are 5.6 and 5.7, respectively. Both creep damage and eutectic reaction get involved in cladding failure in these cases; like the FM2 test result, creep rupture occurs after eutectic penetration. Predicted penetration depths of M2(2) and M3(2) at failure are 86% and 83%, respectively. Predicted axial failure sizes of M2(2) and M3(2) are 0.5 mm and 1.0 mm.

M2(3) and M3(3) test pins are high-burnup (7.9 at%) pins. Initial plenum pressure is 9.23 MPa. Experimental peak P/Fs of M2(3) and M3(3) tests are 4.1 and 3.4, respectively. M2(3) pin was failed and M3(3) pin was not. Predicted P/Fs at failure of M2(3) and M3(3) tests are 4.1 and 3.8. No eutectic penetration was observed in experiment. In these cases, only creep damage is involved in cladding failure, which corresponds with the experimental result. Predicted axial failure sizes of M2(2) and M3(2) are 0.5 mm and 1.0 mm, respectively.

4.3. Result for the test M6

M6 test is simulated experiment of overpower condition with U-19Pu-10Zr fuel and D9 cladding. Two pins with different burnups were exposed to the hypothetical overpower condition simultaneously: 1.9 at% (M6(1)), and 5.3 at% (M6(2)).

M6(1) test pin is low-burnup (1.9 at%) pin. Initial plenum pressure is 1.82 MPa. Cladding failure did not occur in experiment, and peak P/F of M6(1) test is 4.4. Predicted P/F at failure of M6(1) test is 4.4. Cladding failure of M6(1) test in FE analysis is caused by only eutectic penetration, which is similar to M2(1) test. Predicted axial failure size of M6(1) test pin is 20.5 mm.

M6(2) test pin is medium-burnup (5.3 at%) pin. Initial plenum pressure is 5.15 MPa. Experimental P/F at failure of M6(2) test was 4.4 and eutectic reaction was major failure mechanism [4]. Predicted P/F at failure of M6(2) test is 4.3 and predicted eutectic penetration depth is 87%, which corresponds with experimental tendency. Experimental axial failure size of M6(2) test pin is under 3.8 mm, and predicted axial failure size is 1.5 mm.

4.4. Result for the test M7

M7(1) test pin is very high-burnup (9.8 at%) pin with U-19Pu-10Zr fuel and D9 cladding. Initial plenum pressure of M7(1) pin is 10.45 MPa. Experimental P/F at failure is 4.0 and eutectic penetration was observed in experiment [4]; exact penetration depth was not published. The predicted P/F at failure is 4.5, which is higher than the experimental value at failure; similar prediction results are derived using the COBRA/EXP code. Considering extremely high burnup of the M7(1) pin, it is thought that lanthanide induced clad wastage could take place during pre-irradiation, or irradiation induced embrittlement mechanism may be involved, resulting in cladding failure at lower P/F. Cladding failure in simulation arises from only creep damage, because estimated peak temperature

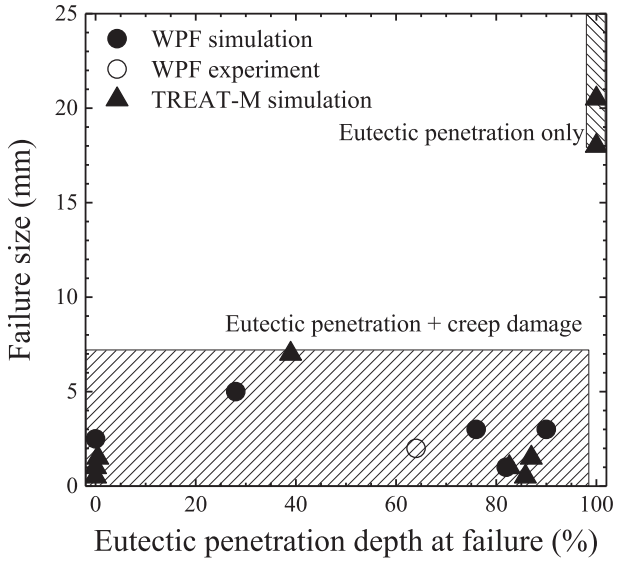

Fig. 6. Predicted and experimental failure size versus eutectic penetration depth at failure.

(1333 K) is lower than eutectic critical temperature (1353 K), as given in Table 8. Predicted axial failure size of M7(1) test pin is 1.5 mm.

M7(2) test pin is low-burnup (2.9 at%) pin with U-10Zr fuel and HT9 cladding. Initial plenum pressure of M7(2) pin is 2.74 MPa. Cladding failure did not occur in experiment. Peak P/F of M7(2) test is 4.8. Predicted P/F at failure is 4.6. In experiment, cladding failure was delayed because of high eutectic critical temperature of U-10Zr fuel; eutectic critical temperature is closely connected with melting temperature [4]. Experimental and predicted penetration depth are 30% and 39%, respectively. Predicted axial failure size of M7(2) test pin is 7.0 mm.

5. Conclusion

This paper presents a fracture simulation of SFR metallic fuel pin using finite element damage analysis method. Major damage mechanisms of metallic fuel pin, creep damage and eutectic penetration are implemented to predict cladding failure using commercial finite element analysis software, Abaqus with user-subroutines. In this simulation method, very fine 2D axisymmetric elements are used to predict accurate failure time, site and size. Use of very fine mesh in nonlinear implicit analysis extremely increases computational burden but it can be treated efficiently using parallel computational method supported by Abaqus.

To validate the proposed simulation method, it is applied to WPF [12–14] (extended transient condition) and TREAT-M [4,15,16] (unprotected overpower condition) tests. Predicted failure time, site and size are compared with experimental failure time, site and size. In WPF and TREAT-M tests, predicted results agree overall well with experimental results. However, for the M7 pins, predicted failure time does not match with experimental failure time possibly due to the long-term aging effect on very high-burnup fuel pin and high eutectic penetration resistance of U-Zr fuel.

The effect of failure mechanisms on failure size is studied in all test cases. Failure size versus eutectic penetration depth at failure is given in Fig. 6. When only eutectic penetration involves in cladding failure, failure size becomes large (over 18 mm). On the other hand, when both eutectic penetration and creep involves in cladding failure, failure size becomes small (under 7 mm).

Declaration of competing interest

The authors declare that they have no known competing financial interests or personal relationships that could have appeared to influence the work reported in this paper.

Acknowledgment

This research was supported by the National Research Foundation of Korea (NRF) funded by the Ministry of Science and ICT. (NRF-2013M2B2B1075733).

Reference

[1] J.E. Cahalan, J.M. Kramer, J.F. Marchaterre, C.J. Mueller, D.R. Pedersen, R.H. Sevy, D.C. Wade, T.Y.C. Wei, Integral Fast Reactor Safety Features, No. CONF-880506-12, Argonne National Laboratory, Argonne, USA, 1988.
[2] K.J. Miles Jr., A.M. Tentner, Metal Fuel Safety Performance, No. CONF-880506-18, Argonne National Lab, Argonne, USA, 1988.
[3] A.M. Tentner, E. Parma, T. Wei, R. Wigeland, Severe Accident Approach - Final Report. Evaluation of Design Measures for Severe Accident Prevention and Consequence Mitigation, No. ANL-GENIV-128, Argonne National Laboratory, Argonne, USA, 2010, https://doi.org/10.2172/973483.
[4] T.H. Bauer, A.E. Wright, W.R. Robinson, J.W. Holland, E.A. Rhodes, Behavior of modern metallic fuel in treat transient overpower tests, Nucl. Tech. 92 (3) (1990) 325–352, https://doi.org/10.13182/NT92-325.
[5] H. Heo, S.D. Park, D.W. Jerng, I.C. Bang, Visual study of ex-pin phenomena for SFR with metal fuel under initial phase of severe accidents by using simulants, J. Nucl. Sci. Technol. 53 (9) (2016) 1409–1416, https://doi.org/10.1080/00223131.2015.1120246.
[6] M.H. Lee, H. Hyo, I.C. Bang, D.W. Jerng, Effect of rupture size in Ex-pin phenomena of severe accident in SFR, in: Proceedings of 2017 International Congress on Advances in Nuclear Power Plants, Fukui and Kyoto, Japan, April 24-28, 2017.
[7] M.H. Lee, H. Hyo, D.W. Jerng, I.C. Bang, Phenomenological study on the Ex-pin phenomena in the initial phase of HCDA on metal-fueled SFR using simulant, Ann. Nucl. Energy 130 (2019) 34–46, https://doi.org/10.1016/j.anucene.2019.02.024.
[8] T. Sofu, J.M. Kramer, The SAS4A/SASSYS-1 Safety Analysis Code System, Chapter 11: FPIN2 Pre-failure Metal Fuel Pin Behavior Model, No. ANL/NE-16/19, Argonne National Laboratory, Argonne, USA, 2017.
[9] A. Biancheria, T.S. Roth, B.E. Sundquist, Steady-state and transient fuel performance modelling: LIFE-4 update, in: Proceedings of International Conference on Reliable Fuels for Liquid Metal Reactors 5.1-5.14, Tucson, USA, September 7-11, 1986.
[10] A. Karahan, Modeling of Thermos-Mechanical and Irradiation Behavior of Metallic and Oxide Fuels for Sodium Fast Reactors, Doctoral thesis, Massachusetts Institute of Technology, Cambridge, USA, 2009.
[11] Dassault Systems, Abaqus Version 2016 Manual, Velizy-Villacoublay, France, 2015.
[12] Y.Y. Liu, H.C. Tsai, D.A. Donahue, D.O. Pushis, F.E. Savoie, J.W. Holland, A.E. Wright, C. August, J.L. Bailey, D.R. Patterson, Whole-pin furnace system: an experimental facility for studying irradiated fuel pin behavior under potential reactor accident conditions, in: Proceedings of ANS Topical Meeting on Fast Reactor Safety 491, Snowbird, USA, August 12-16, 1990.
[13] Y.Y. Liu, H.C. Tsai, M.C. Billone, J.W. Holland, J.M. Kramer, Behavior of EBR-II Mk-V-type fuel elements in simulated loss-of-flow tests, J. Nucl. Mater. 204 (1993) 194–202, https://doi.org/10.1016/0022-3115(93)90217-M.
[14] J.M. Kramer, Y.Y. Liu, M.C. Billone, H.C. Tsai, Modeling the behavior of metallic fast reactor fuels during extended transients, J. Nucl. Mater. 204 (1993) 203–211, https://doi.org/10.1016/0022-3115(93)90218-N.
[15] W.R. Robinson, R.K. Lo, A.E. Wright, T.H. Bauer, G.S. Stanford, J.A. Morman, Integral fast reactor safety tests M2 and M3 in TREAT, in: Proceedings of ANS Winter Meeting, 50, November 10, 1985, pp. 352–353. San Francisco, USA.
[16] W.R. Robinson, T.H. Bauer, A.E. Wright, E.A. Rhodes, G.S. Stanford, A.E. Klickman, First TREAT transient overpower tests on U-Pu-Zr fuel:M5 and M6, Trans. Am. Nucl. Soc. 55 (1987) 418.
[17] N.E. Toredas, M.S. Kazimi, Nuclear Systems: Thermal Hydraulic Fundamentals, CRC press, Boca Raton, USA, 2012.
[18] L. Leibowitz, R.A. Blomquist, Thermal conductivity and thermal expansion of stainless steels D9 and HT9, Int. J. Thermophys. 9 (5) (1988) 873–883, https://doi.org/10.1007/BF00503252.
[19] J.K. Fink, L. Leibowitz, Thermodynamic and Transport Properties of Sodium Liquid and Vapor, No. ANL/RE-95/2, Argonne National Laboratory, Argonne, USA, 1995.
[20] N. Yamanouchi, M. Tamura, H. Hayakawa, A. Hishinuma, T. Kondo, Accumulation of engineering data for practical use of reduced activation ferritic steel: 8%Cr–56-2%W-0.2%V-0.04%Ta-Fe, J. Nucl. Mater. 191 (1992) 822–826, https://doi.org/10.1016/0022-3115(92)90587-B.
[21] A. Banerjee, S. Raju, R. Divakar, E. Mohands, High temperature heat capacity of alloy D9 using drop calorimetry based enthalpy increment measurements, Int.

J. Thermophys. 28 (1) (2007) 97–108, https://doi.org/10.1007/s10765-006-0136-0.
[22] S. Sharafat, R. Amodeo, N.M. Ghoniem, Materials Data Base and Design Equations for the UCLA Solid Breeder Blanket, No. UCLA-ENG-8611/PPG-937, California University, Los Angenles, USA, 1986.
[23] K.J. Miles, The SAS4A/SASSYS-1 Safety Analysis Code System. Chapter 9: DEFORM-5 Metallic Fuel Cladding Transient Behavior Model, No. ANL/NE-16/19, Argonne National Laboratory, Argonne, USA, 2017.
[24] R.J. Dimelfi, J.M. Kramer, Modeling the effects of fast-neutron irradiation of the subsequent mechanical behavior of type 316 stainless steel, J. Nucl. Mater. 89 (1980) 338–346, https://doi.org/10.1016/0022-3115(80)90065-3.
[25] J.M. Kramer, R.J. Dimelfi, Modeling deformation and failure of fast reactor cladding during simulated accident transients, Nucl. Eng. Des. 63 (1) (1981) 47–54, https://doi.org/10.1016/0029-5493(81)90016-9.
[26] Bj Makenas, Swelling of 316 Stainless Steel and D9 Cladding in FFTF, No. ASTM-Stp33814s, American Society for Testing and Materials, Philadelphia, USA, 1987, https://doi.org/10.1520/STP33814S.
[27] T.H. Bauer, G.R. Fenske, J.M. Kramer, Cladding failure margins for metallic fuel in the integral fast reactor, in: Proceedings of International Conference on Structural Mechanics in Reactor Technology, August 17, 1987. Lausanne, Switzerland.
[28] A.B. Cohen, H. Tsai, L.A. Neimark, Fuel/cladding compatibility in U-19Pu-10Zr/HT9-clad fuel at elevated temperatures, J. Nucl. Mater. 204 (1993) 244–251, https://doi.org/10.1016/0022-3115(93)90223-L.
[29] H. Tsai, Fuel/cladding Compatibility in Irradiated Metallic Fuel Pins at Elevated Temperatures. in: Proceedings of ANS Topical Meeting on Fast Reactor Safety 257, Snowbird, USA, August 12-16, 1990.
[30] H.W. Ryu, K.D. Bae, Y.J. Kim, J.J. Han, J.S. Kim, P.J. Budden, Ductile tearing simulation of Battelle pipe test using simplified stress-modified fracture strain concept, Fatig. Fract. Eng. Mater. Struct. 39 (2016) 1391–1406, https://doi.org/10.1111/ffe.12456.
[31] N.H. Kim, C.S. Oh, Y.J. Kim, C.M. Davies, K. Nikbin, D.W. Dean, Creep failure simulations of 316H at 550°C: Part II – effects of specimen geometry and loading mode, Eng. Fract. Mech. 105 (2013) 169–181, https://doi.org/10.1016/j.engfracmech.2013.04.001.
[32] T. Kobayashi, M. Kinoshita, S. Hattori, T. Ogawa, Y. Tsuboi, M. Ishida, S. Ogawa, H. Saito, Development of the SESAME metallic fuel performance code, Nucl. Tech. 89 (2) (1990) 183–193, https://doi.org/10.13182/NT90-A34345.
[33] T. Ogata, T. Yokoo, Development and validation of ALFUS: an irradiation behavior analysis code for metallic fast reactor fuels, Nucl. Technol. 128 (1) (1999) 113–123, https://doi.org/10.13182/NT99-A3018.